HHS Public Access

Author manuscript

Nat Commun. Author manuscript; available in PMC 2015 January 10.

Published in final edited form as:

Nat Commun. ; 5: 4389. doi:10.1038/ncomms5389.

Learning-induced and stathmin-dependent changes in microtubule stability are critical for memory and disrupted in ageing

Shusaku Uchida[1,2,*], **Guillaume Martel**[1,*], **Alice Pavlowsky**[3], **Shuichi Takizawa**[1], **Charles Hevi**[1], **Yoshifumi Watanabe**[2], **Eric R. Kandel**[4], **Juan Marcos Alarcon**[3], and **Gleb P. Shumyatsky**[1]

[1]Department of Genetics, Rutgers University, 145 Bevier Rd., Piscataway, New Jersey 08854, USA

[2]Division of Neuropsychiatry, Department of Neuroscience, Yamaguchi University Graduate School of Medicine, 1-1-1 Minami-Kogushi, Ube, Yamaguchi 755-8505, Japan

[3]Department of Pathology, State University of New York, Downstate Medical Center, 450 Clarkson Ave, Brooklyn, New York 11203, USA

[4]Department of Neuroscience, Columbia University, Howard Hughes Medical Institute, Kavli Institute for Brain Science, 1051 Riverside Dr., New York, New York 10032, USA

Abstract

Changes in the stability of microtubules regulate many biological processes, but their role in memory remains unclear. Here we show that learning causes biphasic changes in the microtubule-associated network in the hippocampus. In the early phase, stathmin is dephosphorylated, enhancing its microtubule-destabilizing activity by promoting stathmin-tubulin binding, whereas in the late phase these processes are reversed leading to an increase in microtubule/KIF5-mediated localization of the GluA2 subunit of AMPA receptors at synaptic sites. A microtubule stabilizer paclitaxel decreases or increases memory when applied at the early or late phases, respectively. Stathmin mutations disrupt changes in microtubule stability, GluA2 localization, synaptic plasticity and memory. Aged wild-type mice show impairments in stathmin levels, changes in microtubule stability, and GluA2 localization. Blocking GluA2 endocytosis rescues memory deficits in stathmin mutant and aged wild-type mice. These findings demonstrate a role for microtubules in memory in young adult and aged individuals.

Correspondence: Gleb P. Shumyatsky, Ph.D. gleb@biology.rutgers.edu.

*These authors contributed equally to this work.

Author Contributions

S.U. and G.M. contributed equally to the work. S.U., G.M., S.T., A.P., J.M.A. and G.P.S. conceived and designed the experiments. S.U. performed the molecular, viral, histological and behavioral experiments. G.M. performed the histological and behavioral experiments. C.H. performed the histological experiments. S.T. and G.P.S. performed the transgenic experiments. A.P. performed the electrophysiological experiments. All of the authors discussed the results and commented on the manuscript. G.P.S. and S.U. wrote the manuscript with input from J.M.A. Y.W. and E.R.K.

Supplementary Information is linked to the online version of the paper at http://www.nature.com/naturecommunications

Competing financial interests: The authors declare no competing financial interests.

Introduction

In the brain, following neuronal activity there is an increase in synaptic transport, which results in the strengthening of synaptic connections, and ultimately in memory formation[1]. Among the many mechanisms mediating synaptic transport, cytoskeletal structures – actin filaments and microtubules – play a major role in motor-driven import and export[2]. Actin filaments are known to be dynamic and present in dendritic spines where they play an essential role in synaptic function and memory formation[3]. Microtubule dynamics have been described in cell division, axonal pathfinding during development, and axonal growth and regeneration. In contrast, in mature neurons, microtubules are generally viewed as stable non-dynamic structures present in dendritic shafts but not in dendritic spines. Intriguingly, recent work in hippocampal primary neuronal cultures indicates that microtubules can also be dynamically regulated during neuronal activity by moving from the dendritic shaft to the dendritic spines and affecting synaptic structure and function[4–9]. Despite this new information, the role of changes in microtubule stability in memory formation remains unclear.

Microtubule assembly from heterodimers of α- and β-tubulins involves interaction with microtubule-associated proteins. One of these proteins, stathmin, binds tubulin heterodimers and prevents microtubule assembly, thus controlling microtubule dynamics[10, 11]. When phosphorylated, stathmin releases tubulin dimers allowing microtubules to be formed[12, 13]. Stathmin has been linked to fear, cognition, and aging in rodent and human studies[14–19], suggesting the involvement of microtubule dynamics in memory.

Therefore, we set out to examine the role of stathmin-regulated control of microtubule stability in memory formation by focusing on learning-induced changes, because activity-dependent signaling is a hallmark of neuronal function[20, 21]. Our approach reveals that, by regulating microtubule stability and dendritic transport of the GluA2 subunit of AMPA-type glutamate receptors (AMPARs), stathmin controls synaptic plasticity and memory consolidation. Furthermore, we observe that aged wild-type mice, in addition to memory deficits, display deficits in stathmin levels, learning-dependent changes in microtubule stability and GluA2 dendritic transport along microtubules. Our combined approach demonstrates that learning-induced and stathmin-mediated changes in microtubule stability control GluA2 dendritic transport, synaptic plasticity and memory formation, pointing to a new learning-dependent intracellular signaling pathway.

Results

Stathmin activity is regulated by learning

We first examined expression of stathmin protein in adult mice and found it to be present in the brain and testis (Supplementary Fig. 1a). In the brain, stathmin is located in the hippocampus, prefrontal cortex, amygdala, striatum, hypothalamus, and cerebellum (Supplementary Fig. 1b). Stathmin is strongly expressed in the dentate gyrus with lesser expression in the CA3 and CA1 (Supplementary Fig. 1c). In the dentate gyrus, stathmin was found not only in the whole-cell extracts, but also in the synaptosomal fraction

(Supplementary Fig. 1d). Based on this observation, we focused our work on the dentate gyrus synaptosomes.

To examine whether stathmin phosphorylation is regulated by learning, synaptosomal fractions from the dentate gyrus were isolated at several time points (5, 15, 30 min, 1, 2, 8, or 24 h) from mice subjected to single-shock contextual fear conditioning. Compared to naïve mice, phosphorylation of synaptosomal stathmin at Ser16, Ser25 and Ser38 was rapidly decreased in mice 15–60 min following fear conditioning training and then phosphorylation of synaptosomal stathmin at Ser16 and Ser38 was increased 8 h following fear conditioning training (Fig. 1a and Supplementary Fig. 2). To confirm that the observed changes were specific to associative learning, we examined the effects of exposure to the context only (no shock) or the immediate shock deficit on stathmin phosphorylation (Supplementary Fig. 3). In mice exposed to context only or to the immediate shock, phosphorylation of stathmin at Ser25 and Ser38 was rapidly decreased 30–60 min following the exposure, but no changes in phospho-stathmin levels were observed at 8 h. In contrast, there was no effect of either the context only or the immediate shock on stathmin phosphorylation at Ser16.

We examined if the changes in stathmin phosphorylation following learning regulate stathmin-tubulin binding, which in turn may affect microtubule stability. Using co-immunoprecipitation on the synaptosomal fractions of the dentate gyrus, we found that stathmin binding to α-tubulin, a major component of microtubules, increased in the first 30 min but decreased the following 8 h after training (Fig. 1b). In mice exposed to context only, stathmin binding to α-tubulin was increased 30 min, but not 8 h, following the exposure (Supplementary Fig. 4). These data suggest that during associative learning, stathmin may regulate microtubule stability, by changing its affinity to α-tubulin.

Changes in microtubule stability following learning

To examine microtubule stability following learning, we measured the levels of the detyrosinated tubulin, a marker of stable microtubules, and tyrosinated tubulin, a marker of labile microtubules[22–24]. We found biphasic changes in tyrosinated and detyrosinated tubulin in the synaptosomal fractions of the dentate gyrus: detyrosinated tubulin levels were decreased 30–60 min and increased 8 h following contextual fear conditioning, whereas tyrosinated tubulin levels were changed in the opposite direction (Fig. 1c and Supplementary Fig. 5). Similar to the changes in stathmin phosphorylation, exposure to context only (Supplementary Fig. 6a) or immediate shock (Supplementary Fig. 6b) led to a reduction of the detyrosinated tubulin and an increase in tyrosinated tubulin 0.5 h, but not 8 h, following the exposure. These results suggest that the increase in microtubule stability at 8 h is specific to associative learning. These results further suggest that microtubules become unstable 0.5–1 h and hyperstable 8 h following learning and the increase in phospho-stathmin and subsequent microtubule hyperstability may be involved in memory consolidation.

Memory can be enhanced by increasing microtubule stability

We investigated whether pharmacological manipulation of the increase in microtubule stability following learning affects memory. We used paclitaxel or nocodazole to stabilize or

destabilize microtubules, respectively. The drugs were injected into the dentate gyrus area of wild-type mice 8 h following fear conditioning and memory was tested 24 h after training (Fig. 1d). Nocodazole injections decreased (Fig. 1e), while paclitaxel injections increased memory (Fig. 1f). To rule out the possibility that nocodazole injections disrupted freezing in a non-associative manner, we injected nocodazole into the dentate gyrus area of wild-type mice in home cage 24 h after they were subjected to contextual fear conditioning (Supplementary Fig. 7). Their freezing responses were measured 48 h after training. There were no differences in freezing between mice injected with nocodazole and vehicle, thus suggesting that the nocodazole treatment alone did not disrupt freezing. These pharmacological experiments demonstrate that memory can be enhanced or disrupted by changing microtubule hyperstability 8 h following learning, and it also suggests that during this time period microtubule-dependent intracellular processes involved in memory consolidation are sensitive to manipulation.

Stathmin controls microtubule stability and LTP

To examine how stathmin-dependent microtubule stability may affect synaptic plasticity and memory, we employed transgenic mice expressing a mutant form of stathmin. *Stathmin4A* double mutant mice (*Stat4A*) were generated using the *tTA/tetO* inducible bi-transgenic system, which allows the *Stathmin4A* transgene to be turned on and off (Fig. 2a). The unphosphorylatable Stathmin4A gain-of-function mutant has its four Ser residue phosphorylation sites changed to Ala. Thus, it irreversibly binds α-tubulin, depleting cellular levels of free tubulin, and thus competing with endogenous stathmin and destabilizing microtubules[25]. Experimental mice were generated by crossing the GRP^{tTA} knockin mouse and *tetO-Stat4A:GFP* transgenic mouse. In the *tetO-Stat4A:GFP* transgenic line, *Stathmin4A* is fused to *GFP* under the control of the tTA-dependent *tetO* transcriptional operator. The *Stat4A:GFP* transgene is transcribed in the presence of tTA when these transgenic mice are crossed with the tTA-expressing line, GRP^{tTA} knockin mouse. Immunohistochemistry and Western blotting revealed that the transgene was expressed in several brain areas, including the hippocampus, medial prefrontal cortex, anterior cingulate gyrus, and amygdala (Supplementary Fig. 8a,b). Within the hippocampus, the *Stat4A:GFP* transgene was strongly expressed in the dentate gyrus (Fig. 2b) where it was present in neurons but not astrocytes (Supplementary Fig. 8c). The expression of the transgene did not affect the gross anatomy of the brain and the cilia in *Stat4A* mice (Supplementary Fig. 8d,e). The *Stat4A:GFP* transgene was expressed in the absence of the drug doxycycline (Fig. 2c; Off dox), but the transgene was turned off within three weeks after the dox was added to the diet (On dox).

We analyzed microtubule stability in the dentate gyrus synaptosomal fraction of *Stat4A* mice following contextual fear conditioning. Western blotting revealed that detyrosinated tubulin levels were decreased 30 min after training in both *Stat4A* and wildtype mice, but *Stat4A* mice did not show an increase in detyrosinated tubulin levels at 8-h time point, thus suggesting improper regulation of microtubule stability (Fig. 2d). Feeding *Stat4A* mice with dox for three weeks rescued the deficit (Fig. 2d). These results indicate that phosphorylation of stathmin is essential for microtubule hyperstability following learning.

We tested synaptic strength and plasticity in *Stat4A* mice. Transgenic mice showed a trend to decrease maximum synaptic responses to afferent stimuli in the perforant path-dentate gyrus synaptic input (Fig. 3a), and a deficient theta-burst-induced long-term potentiation (LTP) (Fig. 3b). In contrast, synaptic strength and LTP at Schaffer collateral-CA1 synapses were normal (Fig. 3c,d). These experiments demonstrate that stathmin-dependent microtubule dynamics are critical for synaptic plasticity in the dentate gyrus.

Context fear memory is dependent on dentate gyrus stathmin

Next, we examined how the deficiency in microtubule hyperstabilization at the 8-h time point might affect memory in *Stat4A* mice. In single-shock contextual fear conditioning, *Stat4A* mice showed a deficit in long-term memory (24 h), which was rescued by dox at the adult stage (Fig. 4a). In contrast, there was no significant difference in short-term memory (0.5 h) in *Stat4A* mice (Fig. 4b). *Stat4A* mice were normal in tone-shock single pairing cued fear conditioning (Fig. 4c), which is dependent on the amygdala but not on the hippocampus. We also examined the role of stathmin in spatial memory using the Morris water maze and Barnes maze. In the Morris water maze test, *Stat4A* mice showed a deficit in initial spatial learning and reversed learning but were normal in the probe test (Fig. 4d–g). In the Barnes maze, we found that the spatial coordinates of the target box was delayed for *Stat4A* mice compared to wildtype control animals (Fig. 4h). The results from these two independent memory paradigms confirm impairment in hippocampus-dependent memory in *Stat4A* mice.

Anxiety tested in the open field and elevated plus maze was normal (Supplementary Fig. 9a–c) in *Stat4A* mice. Also, depression-like behaviors assessed by the forced swim test and sucrose preference tests were normal in *Stat4A* mice (Supplementary Fig. 9d,e). Thus, deficits in stathmin-dependent microtubule stability lead to a decrease in contextual fear memory without affecting cued fear memory, anxiety or depression-like behavior in *Stat4A* mice.

Stat4A mice express the transgene in the dentate gyrus area and have a deficiency in perforant path-dentate gyrus LTP but have a normal Schaffer collateral-CA1 LTP, suggesting that improper dentate gyrus microtubule function may be responsible for the deficits in contextual fear memory. However, transgene expression in the amygdala and some cortical areas may also affect contextual fear conditioning in these mice. To confirm that the deficits in contextual fear conditioning are caused by changes in dentate gyrus microtubules, we overexpressed the *Stathmin4A* transgene in the dentate gyrus of wild-type mice using adeno-associated virus (AAV)-mediated gene transfer (Fig. 5a). The levels of the detyrosinated tubulin in mice injected with *AAV-Stat4A-IRES-GFP* in the dentate gyrus were normal 30 min, but decreased 8 h following learning (Fig. 5b,c). These mice also displayed reduced contextual fear memory compared to control mice injected with *AAV-GFP* (Fig. 5d). These results show that learning-induced and stathmin-dependent changes in microtubule stability in the dentate gyrus are critical for contextual fear memory.

Role of learning-induced microtubule instability in memory

Next, we investigated microtubule instability occurring 0.5 h after learning using paclitaxel injections in the dentate gyrus area of wild-type mice. Because the level of the detyrosinated tubulin in wild-type mice was decreased 0.5–1 h following learning (Fig. 1c), we injected paclitaxel immediately after contextual fear conditioning to inhibit microtubule destabilization. Memory was assessed 24 h following training (Fig. 6a). We found that mice injected with paclitaxel had reduced contextual fear memory.

We also investigated the effect of stathmin loss-of-function mutation on microtubule stability and memory using *stathmin*$^{-/-}$ mice. In contrast to wild-type mice, there were no changes in the detyrosinated and tyrosinated α-tubulin levels in the dentate gyrus synaptosomal fractions in *stathmin*$^{-/-}$ mice 30 min and 8 h following contextual fear conditioning (Fig. 6b). *Stathmin*$^{-/-}$ mice had normal gross brain morphology (Supplementary Fig. 10) and were deficient in contextual fear memory tested 24 h after training (Fig. 6c). These data indicate that in the absence of stathmin, both early instability and late hyperstability in microtubules are deficient following learning, leading to deficits in memory formation.

Stathmin regulates learning-dependent GluA2 localization

Which downstream events are regulated by stathmin-dependent changes in microtubule stability? Microtubules in dendrites of mature neurons are mainly responsible for intracellular transport[2]. Learning-induced AMPA-type glutamate receptors are delivered to spines in the hippocampus, which are critical for synaptic plasticity[26] and contextual memory[27, 28]. Principal neurons in the adult brain express AMPARs that predominately contain the GluA2 subunit[29]. Therefore, we injected *AAV-Stat4A-IRES-GFP* in the dentate gyrus to examine whether learning-induced intracellular transport of GluA2 along dendrites is regulated by stathmin-dependent changes in microtubule stability. The amount of GluA2 in the dentate gyrus synaptosomal fractions of wild-type mice injected with the control *AAV-GFP* virus significantly increased 8 h after contextual fear conditioning, whereas mice injected with the *AAV-Stat4A-IRES-GFP* did not show an increase in GluA2 (Fig. 7a). GluA2 levels were the same in the whole-cell extracts from mice injected with the *AAV-GFP* or *AAV-Stat4A-IRES-GFP* (Fig. 7b), suggesting that an increase in GluA2 levels in the synaptosomal fractions after learning might be caused by enhanced dendritic transport from the soma to the dendritic shaft along the hyperstable microtubules. Indeed, the GluA2 levels in the microtubule fractions were significantly increased after training in control mice injected with the *AAV-GFP*, whereas mice injected with *AAV-Stat4A-IRES-GFP* did not show increased GluA2 (Fig. 7c).

Next, we examined if learning induces changes in the GluA2 levels in *stathmin*$^{-/-}$ mice. In contrast to wild-type mice, *stathmin*$^{-/-}$ mice did not show an increase in the GluA2 levels in the synaptosomal fractions at the 8-h time point (Fig. 7d). The GluA2 levels were normal in the whole-cell extracts in *stathmin*$^{-/-}$ mice (Fig. 7e). Similar to the synaptosomal fraction, the GluA2 levels in the microtubule fraction were not increased 8 h following training in *stathmin*$^{-/-}$ mice, whereas wild-type mice showed an increase in the GluA2 levels (Fig. 7f).

These results suggest that learning promotes GluA2 localization to the synaptic sites in stathmin- and microtubule-dependent manner.

To examine whether synaptic GluA2 levels are also altered by stathmin mutation, we investigated GluA2 localization by fractionation of synaptosomes. We performed further digestion of synaptosomes to yield an insoluble "PSD-enriched" membrane fraction and a "non-PSD enriched" membrane fraction (Supplementary Fig. 11)[30, 31]. We found increased GluA2 in both the synaptic PSD and non-PSD fractions in wild-type mice 8 h after learning, whereas there was no difference in the GluA2 levels either in the PSD and non-PSD fractions from the wild-type mice injected with the *AAV-Stat4A-IRES-GFP* as well as from *stathmin*$^{-/-}$ mice (Supplementary Fig. 12).

We also examined whether disruption of learning-induced microtubule hyperstability influences increase in synaptosomal and synaptic GluA2. Wild-type mice were injected with nocodazole 2 h after contextual fear conditioning and were euthanized 8 h after training (Supplementary Fig. 13a). We found increased GluA2 levels in PSD and synaptosomal fractions, but not in whole cell extracts, in vehicle treated mice (Supplementary Fig. 13b). However, we did not find an enhancement of the GluA2 levels either in the PSD or synaptosomal fractions in nocodazole-treated mice (Supplementary Fig. 13b). These results further confirm that changes in microtubule stability following learning are critical for synaptosomal and synaptic localization of GluA2.

Stathmin-dependent binding of KIF5 to microtubules and GluA2

We further investigated how stathmin regulates dendritic GluA2 localization following learning. Tubulin detyrosination (a marker of stable microtubules) induces kinesin motor protein KIF5 binding to microtubules as well as its motor activity[32]. Moreover, in dendrites, GluA2 is transported by KIF5[33]. This led us to speculate that learning-induced tubulin detyrosination activated both KIF5 binding to microtubules and KIF5-dependent GluA2 transport. We performed co-immunoprecipitation to examine the binding of GluA2 to KIF5, KIF5 to α-tubulin, and GluA2 to α-tubulin in the hippocampus after contextual fear conditioning. After training, the binding of GluA2 to α-tubulin, KIF5 to α-tubulin, and KIF5 to GluA2 was increased in wild-type mice but not in *stathmin*$^{-/-}$ mice (Fig. 8a–c), suggesting that KIF5 may be a molecular link which connects stathmin and microtubules to activity-dependent dendritic transport of GluA2.

Blocking GluA2 endocytosis rescues memory deficits

To further examine the role of stathmin-mediated dendritic transport of GluA2, we decided to examine whether increasing the amount of GluA2 at the synapse would rescue contextual fear memory in *stathmin*$^{-/-}$ mice. A synthetic peptide TAT-GluA2$_{3Y}$, known to inhibit GluA2 endocytosis without decreasing basal synaptic transmission or LTP[34], was injected in the dentate gyrus area. This peptide has an estimated half-life time 250–300 min after intravenous injection[34]. To increase the time of its action, we injected the peptide twice, 1 h before and 4 h after training (Fig. 8d). There was no significant difference in freezing between wild-type mice injected with either the TAT-GluA2$_{3Y}$ or TAT-control peptides (Fig. 8e). However, freezing of *stathmin*$^{-/-}$ mice injected with the TAT-GluA2$_{3Y}$ was

significantly increased compared to *stathmin*$^{-/-}$ mice injected with the TAT-control peptide (Fig. 8e).

We also examined if the TAT-GluA2$_{3Y}$ peptide had an effect on contextual fear memory in wild-type mice injected with *AAV-Stat4A-IRES-GFP*. The freezing response in mice injected with *AAV-Stat4A-IRES-GFP* and TAT-GluA2$_{3Y}$ peptide was significantly increased compared to mice injected with *AAV-Stat4A-IRES-GFP* and TAT-control peptide (Fig. 8f). Thus, blocking GluA2 endocytosis rescued memory both in *stathmin*$^{-/-}$ mice and wild-type mice injected with *AAV-Stat4A-IRES-GFP*. This suggests that GluA2 synaptic localization in the dentate gyrus is at least partially mediated by stathmin-dependent microtubule dynamics, and this process is critical for contextual fear memory.

Stathmin-microtubule connection to aged-related memory loss

Previous work implicated stathmin in aging in healthy humans[18]. Furthermore, the dentate gyrus is vulnerable to the effects of normal aging in humans and primates[35, 36]. Indeed, aged mice showed reduced contextual fear memory (Fig 9). We therefore examined stathmin-microtubule interactions in age-dependent memory loss. Intriguingly, similar to the work in humans, we found that stathmin expression in the dentate gyrus of the hippocampus gradually decreased from 2 to 12 to 18 months in naïve wild-type mice (Fig. 10a). We analyzed post-translational modifications of α-tubulin following contextual fear conditioning in the synaptosomal fractions of the dentate gyrus of 18-months-old mice. In contrast to young adult mice, aged mice showed a significant attenuation of changes in detyrosinated tubulin (Fig. 10b), suggesting improper regulation of microtubule stability. Next, we measured GluA2 levels in mice subjected to contextual fear conditioning with one or three foot shocks, and found a significant difference between young adult and aged mice. The GluA2 levels in the dentate gyrus synaptosomal and microtubule fractions were not increased in aged mice after training (one foot shock) (Fig. 10c–e). Furthermore, the aged mice needed a stronger stimulus to reach the levels of GluA2 found in the young adults. To confirm whether the deficit in synaptosomal GluA2 in trained aged mice causes memory deficits, we analyzed contextual fear memory after injecting TAT-GluA2$_{3Y}$ peptide into the dentate gyrus area of aged mice. We found that TAT-GluA2$_{3Y}$ rescued fear memory of aged mice to the level of young adults that received the TAT-control peptide (Fig. 10f). Thus, stathmin-dependent microtubule stability is involved in both regulating memory consolidation in young adult mice and in aged-associated memory loss, suggesting that stathmin-microtubule interactions represent a general mechanism for memory formation.

DISCUSSION

Our work demonstrates that learning induces biphasic changes in stathmin phosphorylation which trigger changes in stathmin-tubulin binding and microtubule stability, leading in turn to increases in GluA2 localization at the synaptic sites, promoting synaptic plasticity and long-term memory. On the other hand, perturbations of the stathmin's function to control microtubule stability lead to deficits in GluA2 localization, synaptic plasticity and memory formation. We found a decrease and then a subsequent increase in stathmin phosphorylation 15 min – 0.5 h (early phase) and 8 h following learning (late phase). Although

phosphorylation of stathmin at all Ser residues is important for inactivation of its depolymerization activity[37, 38], phosphorylation at Ser16 strongly reduces the binding affinity of stathmin to tubulin heterodimers[12, 13, 39]. Ser16 can be phosphorylated by PKA and CaMKII/IV[40–42], the kinases critically involved in memory formation[43–45]. Thus, it is highly likely that the kinases and phosphatases controlling stathmin phosphorylation may have an important role in memory formation by controlling microtubule stability.

We found two distinct phases of changes in microtubule stability: 0.5–1 h following learning when microtubules become unstable (early phase) and 8 h following learning when microtubules become hyperstable (late phase). These results are based on the measurements of microtubule stability using antibodies against tyrosinated and detyrosinated tubulin. While these measurements assess microtubule stability indirectly, they have been used in a number of studies including those when testing of stathmin-dependent microtubule stability in brain tissue was analyzed[24, 46]. Biphasic changes in stathmin-tubulin binding, just like changes in stathmin phosphorylation, provide further support to the notion that microtubules change their stability. Importantly, local injections of a microtubule stabilizing drug paclitaxel at the early phase disrupt, whereas injections at the late phase enhance, long-term memory. Microtubule hyperstability during the late phase appears to be specifically related to associative learning (context-US presentation) because this change is not seen after exposure to context only or immediate shock. In contrast, the early phase changes occur not only after context-US but also after exposure to context only or immediate shock. Thus, the early phase seems to be involved in attention/arousal/US-related events as well as associative memory. It is important to note that manipulating microtubule stability at the early phase also disrupts memory, suggesting that the early phase is necessary for memory formation. We speculate that during the early phase, initial microtubule disassembly caused by increased stathmin activity is likely to trigger subsequent assembly of new microtubules, which are then stabilized during the late phase allowing an increase in dendritic transport.

Our work in live animals suggests that stathmin-dependent changes in microtubule stability are involved in synaptic function and memory formation. The learning-dependent changes in microtubule stability we observed are in agreement with activity-dependent changes in microtubules found at the synapse in hippocampal primary cell cultures[4–9]. Although our data are supported by other literature suggesting that microtubule function is important for memory formation[47–49], its molecular mechanisms remain to be elucidated. Our data provide the mechanism of how learning-induced stathmin phosphorylation regulates microtubule stability and long-term memory formation. In particular, our work is in agreement with Fanara et al.[49] whose study implicates microtubule turnover in learning. A recent study has shown that the levels of stathmin mRNA and protein are increased two days following contextual fear conditioning[50]. It is possible that the increases in stathmin levels found in that paper reflect the compensational changes caused by the earlier use of stathmin on day one following learning as our work demonstrates. These findings are in agreement with our work showing that learning induces changes in stathmin in the dentate gyrus. We found the phospho-stathmin levels to be decreased 30 min and then increased 8 h following training; there were no differences in total stathmin levels at these time points. We also found the levels of total and phospho-stathmin to be normal 24 h following training. Although both studies used single-shock contextual fear conditioning, we still cannot

exclude that the differences in the results may reflect the specific details of the training paradigms.

We showed that stathmin-mediated control of microtubule stability regulates the binding properties of the GluA2-KIF5 motor protein complex and dendritic GluA2 localization. Our observations of enhanced tubulin detyrosination and increased interactions of KIF5 and α-tubulin occurring 8 h following learning are in agreement with the finding in the hippocampal primary cell cultures that tubulin detyrosination enhances the motor activity of KIF5 and its binding to microtubules[32]. We also found that KIF5-GluA2 interactions and synaptosomal and synaptic (PSD fractions) GluA2 levels were increased 8 h following learning. However, *stathmin* mutant mice have deficits in learning-induced GluA2-KIF5 interactions and synaptosomal and synaptic GluA2 localization. KIF5 is known to control intracellular transport of AMPARs[33], and the insertion of AMPARs into spines during synaptic plasticity requires a myosin motor protein[26, 51]. Given the fact that the GluA2 levels in the non-PSD fractions were also deficient in *stathmin* mutant mice, the deficiency in synaptic GluA2 localization in *stathmin* mutant mice might be caused by dysregulation of GluA2 transport from the soma to the dendritic shaft along microtubules. However, synaptic transport can also be deficient as a recent study has shown that KIF5 regulates synaptic delivery and redistribution of AMPARs[52]. Although the molecular mechanisms of synaptic AMPARs delivery are still unclear, our data suggest that stathmin regulates dendritic transport of GluA2 by regulating microtubule stability during memory formation. The ability of the blocker of GluA2 endocytosis to rescue contextual fear memory in *stathmin* mutant mice is in agreement with the role of AMPAR transport in synaptic plasticity and contextual memory[26–28, 53–55]. Therefore, GluA2 intracellular localization at the synaptosomes is controlled by changes in microtubule stability in a learning-dependent manner and these interactions serve as a molecular link to synaptic function and memory formation.

Consistent with stronger expression of both the endogenous stathmin and Stathmin4A transgene in the dentate gyrus compared to other areas of the hippocampus, we found that perforant path-dentate gyrus LTP, but not Schaffer collateral-CA1 LTP, is deficient in *Stat4A* mice. Furthermore, wild-type mice expressing virus-mediated Stathmin4A in the dentate gyrus showed deficiency in contextual fear memory. Taken together, these results demonstrate an essential role of stathmin-microtubule interactions in dentate gyrus synaptic plasticity and contextual fear memory. The timing of the changes of stathmin phosphorylation that we observed in brain sections is different from the timing of LTP induction. One possibility is that learning in live animals and LTP induction in slices may be dependent on somewhat different molecular mechanisms. Other possibilities include changes in localization of certain synaptic molecules in naïve condition that lead to a deficit in LTP induction in *Stat4A* mice. Although our data suggest that dysregulation of dendritic transport of GluA2 in stathmin mutant mice is observed only following learning, we cannot exclude the possibility that stathmin regulates dendritic localization of other molecules even in naïve conditions. Some of the candidates can include kinesin motor proteins as well as their cargo[56].

How general is this signaling pathway for memory formation? To begin answering this question, we turned to aging-associated memory loss focusing on the dentate gyrus, as it is implicated in normal aging in humans and primates[35, 36]. Interestingly, stathmin expression in the human brain is decreased with aging[18] and this decrease is accelerated in Alzheimer's disease[18, 57, 58]. We found that aged mice show decreased stathmin levels and lack of learning-induced increase in GluA2 levels in synaptosomal and microtubule fractions. Furthermore, blocking the GluA2 endocytosis reverses the deficits in contextual fear memory in aged mice, suggesting that the GluA2 dendritic transport has an important role in age-dependent memory loss. This is consistent with a recent report showing that reduced levels of the synaptic GluA2 in the dentate gyrus are associated with memory loss in aged monkeys[59].

In conclusion, our data demonstrate that learning-dependent regulation of GluA2 dendritic transport by stathmin-mediated changes in microtubule stability is crucial for memory formation and dysfunction in this signaling pathway might be one of the mechanisms underlying age-dependent memory loss. Thus, changing stathmin activity or microtubule stability might be a useful approach to regulate memory formation. Given that improving microtubule stability was proposed as an approach to establishing axonal and synaptic connections in spinal cord injury and central nervous system lesions[47, 60, 61], controlling microtubule stability may be a convergent pathway for different biological processes of the nervous system.

Methods

Animals

Male C57BL/6J mice were purchased from Jackson Laboratory. Generation of the *GRP^{tTA}* knock-in mice: The portion of the mouse *Grp* gene 4.5 kb long that includes exon 1 was isolated and the NotI-AscI site inserted in front of the ATG in exon 1, generating a plasmid pGP109(NA). The humanized *htTA* gene (gift from Dusan Bartsch) was inserted into the plasmid pnCreFNF14.19 (after removing nCre cDNA; gift from Xiaoxi Zhuang), generating ptTAFNF. A plasmid pGP109-tTA-FNF was generated by inserting tTA-FNF into the NotI-AscI site of the pGP109(NA). Wild-type and mutant *Grp* alleles were detected using: GRP Forward, 5′-GGACAACGCACTCTCAGCCTAGT-3′; GRP WT Reverse: 5′-GAGACGGGGCTCCCTCTAGCTAG-3′; and GRPtTA Reverse: 5′-AGTCGACCTTGCGCTTCTTCTT-3′. Generation of the *tetO-Stat4A:GFP* transgenic mice: The human *Stathmin4A* cDNA (gift from Andre Sobel) was fused with GFP cDNA and inserted into pMM400 (gift from Mark Mayford). Genotyping was performed with: tetO Forward: 5′-GGTCCAACTGCAGCCCAAGC-3′; WT FW4838: 5′-AGCCTAGCTGTTCTCAGCCCCA-3′; WT Reverse: 5′-GGGTCTTTGGATTCTTTGTTCTTCCG-3′. *Stat4A* mice: Wild-type and double mutant mice were generated by breeding *GRP^{tTA}* with *tetO-Stat4A:GFP* mice. *Stathmin$^{-/-}$* mice were maintained on C57BL/6J background (N>10). All mice were maintained on a 12-hour light/dark cycle in groups of 4–5 per cage. Behavioral experiments were conducted during the light phase of the cycle. Mice were 2–4 months (for young adult), 12 months (for middle-aged) or 16–20 months old (for aged) at the time of the experiments. This study was

carried out in a strict accordance with the recommendations in the Guide for the Care and Use of Laboratory Animals of the National Institutes of Health. The Rutgers University Institutional Animal Care and Use Committee approved the protocol.

Contextual fear conditioning

For single foot-shock contextual fear conditioning [17], on the training day, a mouse was placed in the conditioning chamber (Med Associates) for 148 s before the onset of 2 s of the foot-shock (0.75 mA). After an additional 30 s in the chamber, the mouse was returned to its home cage. 30 min or 24 h after training, freezing was assessed for 3 min by FreezeView software (Coulbourn Instrument). For three foot-shock contextual fear conditioning, the mouse was placed in the conditioning chamber for 300 s during which the mouse received three foot-shock (0.75 mA, 2 s) with the intertrial interval around 58 s. Before the onset of the first US, the mouse was allowed to explore the box for 148 s. After the last US, the mouse stayed in the box additional 30 s before returning to its home cage. Testing was carried out 24 h later, as described above.

Cued fear conditioning

For single-shock cued fear conditioning[62], on the training day, a mouse was placed in the conditioning chamber for 2 min before the onset of the CS, a tone that lasted for 30 s at 2800 Hz, 85 dB. The last 2 s of the CS was paired with the US, 0.75 mA of continuous foot-shock. After additional 30 s in the chamber, the mouse was returned to the home cage. Twenty-four hours after the training, mice were placed in an unfamiliar chamber in which the tone (120 s) that had been presented during training was given after a 1 min habituation period (pre-CS). The freezing response was assessed as described above.

Morris water maze

The task was composed of three training phases[63, 64]. The first phase consisted of two days of training a mouse to reach a visible platform followed by the second phase consisting of four days of training to find a hidden platform. A probe trial was performed on the fifth day, 24 h before starting the third phase consisting of a transfer task with a hidden platform located in the quadrant opposite to the location of the platform during the spatial phase. For each phase, four trials, 90 s maximum with a 15-min inter-trial interval (ITI), were given daily. If the mouse found the platform, it was allowed to rest on it for 20 s before being removed from the pool and placed back into its home cage. If the mouse did not locate the platform within 90 s, the animal was hand guided to it. The animals' trajectories were recorded with a video tracking system (HVS Image Analyzing VP-118).

Appetitive Barnes maze

A modified version of the original task[65] was used in which a mouse had to find the recessed chamber under one of the holes (target box) in order to received food. A circular paltform (90 cm) with 40 holes (hole diameter 5 cm) along the perimeter was used. Mice learned the spatial location of the target box during 4 days of training. Four trials of 300 s maximum with a 30-min ITI interval were given daily. If the mouse found the target box, 5 pellets (millet seeds) were given inside the target box. If a mouse did not find the platform

within 300 s, the animal was hand guided to it and 5 pellets were given. For this task, the food ration was adjusted individually in order for the mice to reach 82% of their ad libitum weights.

Open field test

The open-field [62] consisted of a white arena (43.2 cm × 43.2 cm × 40 cm) coupled to an automated video tracking system (Open Field Activity Software, Med Associates). A mouse was placed in the periphery of the arena, and the time spent in the center of the arena and the total path length were measured. Results were expressed as the percent of the time spent in the center over the total time spent in the arena.

Elevated plus maze

The elevated plus maze[62](1 m above the floor) consisted of a center platform (10 cm × 10 cm), two open arms (40 cm × 10 cm), and two closed arms (40 cm × 10 cm) within walls (height 30 cm). A mouse was placed in the center of the apparatus and the time spent in each arm was measured for 5 min using Limelight software (Coulbourn Instruments). Results were expressed as the percent of the time spent in open arms over the total time spent in the maze.

Forced swim test

A mouse was placed[66] in the water tank (24 cm high × 19 cm in diameter filled with 23–25 °C water to a depth of 15 cm) for 5 min, and the total duration of immobility (i.e., the time during which the animal made only the small movements necessary to keep its head above water) was measured.

Sucrose preference test

A mouse was habituated to drink water from two bottles for 7 d[67]. Then it was subjected to 48 h of forced exposure to 1% sucrose solution to avoid neophobia. Mice were subjected to water deprivation for 16 h before the sucrose preference test was performed. Two pre-weighed bottles, one containing tap water and the other containing 1% sucrose solution, were presented to each animal for 4 h. The position of the water and sucrose bottles (left or right) was switched every 2 h. The bottles were weighed again, and the weight difference represented the animal's intake from each bottle. The sum of water plus sucrose intake was defined as the total intake, and sucrose preference was expressed as the percentage of sucrose intake relative to the total intake.

Immunohistochemistry

Mice were anesthetized with avertin (250 mg/kg i.p.) and perfused with 4% paraformaldehyde (PFA) in 1 × PBS. Their brains were post-fixed overnight in 4% PFA and cryoprotected in 30% sucrose in 1 × PBS. The brains were sectioned (30 μm) using a cryostat, and single or double labeling immunohistochemistry was performed. Primary antibodies included the mouse monoclonal antibodies against NeuN (1:1000, Millipore) and GFAP (1:500, Millipore) and the rabbit polyclonal antibodies against GFP (1:500, Invitrogen) and adenylate cyclase III (1:100, Santa Cruz). Secondary antibodies were

conjugated with Alexa Fluor 488 or 568 (1:500, Molecular Probes) or Cy3 (Jackson ImmunoResearch). Images were acquired using an LSM 510 META laser confocal microscope (Zeiss).

Subcellular fractionation

The dentate gyrus was isolated[68] and for whole tissue lysates, freshly dissected tissues were homogenized in ice-cold RIPA buffer (50 mM Tris, pH 8.0, 1% TritonX-100, 0.1% SDS, 150 mM NaCl) containing protease and phosphatase inhibitor cocktail tablets (Roche Applied Science). Synaptosomal, PSD and non-PSD fractions were isolated using protocol[17, 30, 31] with minor modifications. In brief, pooled dissected tissues from the dentate gyri of 3–4 mice were homogenized in cold buffer containing 0.32 M sucrose, 50 mM sodium fluoride and 10 mM HEPES, pH 7.4. Homogenates were cleared two times at 1,000g for 10 min to yield the nuclear enriched pellet and the S1 fraction. To obtain S2 fraction, the S1 fraction was centrifuged and the supernatants (microsomes and cytosol) were collected. To obtain the synaptosomal fraction, the S1 fraction was passed through a nitrocellulose filter (5 μm, Millipore) and spun at 1000g for 20 min. The synaptosomal pellet was rinsed twice (4 mM HEPES, 1 mM EDTA, pH7.4, 20 min at 12,000g). The resulting pellet was incubated in 20 mM HEPES, 100 mM NaCl, 0.5% Triton X-100, pH7.2 for 15 min and centrifuged. The supernatant (triton-soluble NP fraction) containing non-PSD membranes was retained. The pellet was resuspended in buffer containing 20 mM HEPES, 0.15 mM NaCl, 1% Triton X-100, 1% deoxycholic acid, 1% SDS, pH 7.5 for 1 h and centrifuged at 10,000*g* for 15 min. The supernatant contained the PSD or Triton-insoluble fraction. Nuclear fraction was isolated as previously reported[30], the nuclear-enriched pellets were solubilized in 200 μl nuclear buffer containing 10 mM HEPES/KOH, 10 mM KCl, 10 mM EDTA, 1.5 mM $MgCl_2$, 0.2% BSA, 1 mM DTT, 0.4% NP40, protease and phosphatase inhibitors, followed by gentle rotating. Samples are centrifuged and the pellets retained as the crude nucleus fraction. Pellets were washed with 500 μl nuclear buffer, followed by centrifugation. Pellets were solubilized (20 mM HEPES/KOH, 400 mM NaCl, 1 mM EDTA, 10% Glycerol, 1 mM DTT, protease and phosphatase inhibitors) followed by gentle vortexing. Samples were gently rotated, vortexed (3 s) and centrifuged to yield the nuclear extract (supernatant) and the nuclear envelope (pellet). Microtubule fractionation was performed as previously reported[17]. In brief, the pooled dissected tissues from the dentate gyrus of 3–4 mice were homogenized in 400 μl of microtubule stabilizing buffer MTSB (0.1 M PIPES [pH 6.9], 2 M glycerol, 5 mM $MgCl_2$, 2 mM EGTA, 0.5% Triton X-100, 4 μg ml^{-1} Paclitaxel, 5 μg ml^{-1} pefabloc SC, 5 μg ml^{-1} leupeptin) and ultracentrifuged at 32,000g for 20 min at 4 °C. The resulting pellet was re-suspended in the MTSB buffer. All buffers were supplemented with protease and phosphatase inhibitors (Roche Applied Science). Protein concentration was measured by BCA protein assay (Thermo Scientific).

Western blotting

Western blotting was performed[67, 69] with equal amount of proteins separated on 7% or 12% Bis-Tris gels (Life Technologies), and transblotted onto polyvinylidene difluoride membranes (GE Healthcare Bio-Sciences). Antibodies were against stathmin (1:5000; kindly provided by Dr. A. Sobel), phospho-stathmin (S16, S25, S38) (1:1,000, kindly provided by Dr. A. Sobel), tyrosinated tubulin (1:2,000, Sigma), detyrosinated-tubulin

(1:5,000, Millipore), α-tubulin (1:5,000, Sigma), β-actin (1:5,000, Sigma), GAPDH (1:5,000, Millipore), GM130 (1:2,000, Sigma), Histone H4 (1:2,000, Abcam), SNAP25 (1:2,000, Sternberger Monoclonals), Neuroligin1 (1:1,000, Synaptic Systems), synaptophysin (1:4,000, Sigma), GFP (1:1,000, Life Technologies), GluA2 (1:500, Millipore), KIF5 (1:2,000, Millipore), GluN1 (1:500, Millipore), GluN2A (1:500, Millipore), GluN2B (1:500, Millipore), or PSD95 (1:1,000, Millipore). After incubation with appropriate horseradish peroxidase-conjugated secondary antibodies (HRP-linked anti-mouse IgG or HRP-linked anti-rabbit IgG antibody, Cell Signaling), the blots were developed using the ECL-Plus detection Kit (GE Healthcare Bio-Sciences or Thermo Scientific). When the phospho-specific antibodies were used, all buffers included sodium fluoride (50 mM). Densitometric analysis was performed by ImageQuant software (GE Healthcare) after scanning (Typhoon, GE Healthcare). Each experiment was independently repeated at least two times. Full scans of all Western blots are provided in Supplementary Figures 14 and 15.

Immunoprecipitation

Immunoprecipitation was performed[67] using the synaptosomal fraction from the pooled dissected tissues from the dentate gyrus of 4–5 mice (for Figures 1b and Supplementary Figure 4) or pooled whole cell lysate from the hippocampus of 2–3 mice (for Figure 8a–c) were used for the immunoprecipitation experiments. The lysates (1–2 mg of protein) were precleared with Protein G Plus Agarose beads (Thermo Scientific) and with 2–5 μg of anti-α-tubulin (Sigma), anti-KIF5 (Millipore), or normal mouse IgG antibodies (Santa Cruz Biotechnology), followed by incubation with Protein G Plus Agarose beads. The beads were washed 5 times with RIPA buffer. Proteins were eluted with a sample buffer containing 1% SDS. Western blot analyses of the immunoprecipitated anti-α-tubulin, anti-KIF5, and normal mouse IgG samples and the input (from the precleared step) samples were performed with anti-stathmin, anti-GluA2, anti-KIF5, anti-α-tubulin, or anti-actin antibodies as described above. HRP-conjugated horse anti-mouse IgG antibody (Cell Signaling), HRP-conjugated goat anti-rabbit IgG antibody (Cell Signaling), or HRP-conjugated goat anti-mouse IgG light chain specific antibody (Jackson ImmunoResearch) were used as secondary antibody.

Surgery

Mice were anesthetized with avertin (250 mg/kg) and stainless steel guide cannulae (28 gauge, Plastics One) were implanted into hippocampus (−2.0 mm AP, ±1.5 mm ML, −2.0 mm DV[70]). Seven days after surgery, mice were subjected to the experiments. For drug infusion of C57BL/6J mice injected with AAV (Figure 8f), we carried out two surgeries: first, we injected the *AAV-GFP* or *AAV-Stat4A-IRES-GFP* (see *AAV Work*), then performed cannula surgery at least 2 weeks after the AAV virus was expressed.

Drug and peptide injection

Paclitaxel and nocodazole (Sigma) were used in 5% hydroxypropyl β-cyclodextrin vehicle (wt/vol), at concentrations 10 nM and 30 nM, respectively. Drugs were fused (0.5 μl/hemisphere) through the cannula at a rate 0.1 μl min^{-1}. At the end of experiments, we

confirmed the injection site by injecting 0.5 μl of methylene blue solution bilaterally, followed by histological analysis of coronal brain slices. Mice that did not receive symmetrical and bilateral injections in the dentate gyrus region of the dorsal hippocampus were excluded from the study. Doxycycline (dox, 40 mg kg^{-1}, Bio-Serv) was given to mice (2 months of age) for three weeks to fully repress the transgene expression. TAT-$GluA2_{3Y}$ (TAT-^{869}YKEGYNVYG^{877})[34] or TAT-only control peptides (GenScript) at 15 pmol per side in a volume of 0.5 μl saline were bilaterally infused into the dorsal hippocampus. Surgery and cannulae implantation were done as described above. Cannula placement was verified histologically and only mice with adequate cannula replacement were included in subsequent data analysis.

AAV work

AAV-mediated gene transfer was performed[66, 67] using plasmid DNAs *pAAV-MCS* (CMV promoter, Stratagene) carrying *Stat4A-IRES-GFP* or *GFP* cDNA. AAV viruses (serotype 2) were generated and purified in Vector Biolabs. The genomic titer of each virus was determined using real-time-PCR. For virus injections, mice were anesthetized intraperitonealy with avertin (250 mg kg^{-1}) and placed in a stereotaxic frame. The skull was exposed, and a small portion of the skull over dorsal hippocampus was removed bilaterally with a drill. Subsequently, AAV vectors (1.0×10^{12} viral genomes ml^{-1}) dissolved in physiological saline were injected bilaterally into the dorsal dentate gyrus (AP: −2.0 mm, ML: ±1.2 mm, DV: −2.0 mm [0.25 μl volume] and −2.4 mm [0.25 μl volume] from Bregma[70]) at rate of 0.1 μl min^{-1}. The needle was slowly withdrawn after 3 min. Mice were allowed to recover for 3 weeks after surgery and then subjected to fear conditioning. Successful transduction of the dentate gyrus region was confirmed histologically by immunohistochemistry with GFP. Only mice with strong bilateral GFP expression in target region were included in subsequent data analysis.

Electrophysiology

Hippocampal slice preparation: Transverse hippocampal slices (400 μm) were obtained from adult (2–3 months old) *Stat4A* and wild-type littermate mice. All procedures were performed in compliance with the Institutional Animal Care and Use Committee of the State University of New York, Downstate Medical Center. Slices were cut in ice cold artificial cerebrospinal fluid (ACSF containing: (mM) 119 NaCl, 4.0 KCl, 1.5 $MgSO_4$, 2.5 $CaCl_2$, 26.2 $NaHCO_3$, 1 NaH_2PO_4 and 11 Glucose saturated with 95% O_2, 5% CO_2) and then warmed in oxygenated ACSF to 35 °C for 45 min. Slices were thereafter allowed to equilibrate for at least 60 min in oxygenated ACSF at room temperature. For experiments, slices were immersed in a submerged recording chamber subfused with oxygenated ACSF at 35–36 °C. Field recordings: Field excitatory postsynaptic potentials (fEPSP) from the dentate gyrus area were obtained via stimulation with bipolar electrodes (FHC & Co, ME, USA) and recording with borosilicate glass pipettes (5–10 mΩ) filled with ACSF solution. Responses from perforant pathway to granule cell synapses were obtained with a pair of stimulation and recording electrodes located in the dentate gyrus stratum moleculare. For activation of the Schaffer collateral to CA1 synaptic input, stimulation and recording electrodes were placed in the stratum radiatum of the CA1 area. Test pulse intensity was set at approximately 40% of the maximum fEPSP slope. Test sampling was 0.017 Hz (once per minute) and test pulse

duration was 50 μs. LTP was induced by theta burst stimulation (TBS): three bursts spaced by 20 s, each burst consisting of six trains of high frequency stimulus (6 pulses at 100 Hz) delivered at 10 Hz.

Statistical analysis

Protein expression was determined using one-way ANOVAs with Dunnett's tests. Differences in protein expression between groups were determined using one-way ANOVA or two-way ANOVA, with Fisher's LSD post hoc tests. The behavioral data were examined using a Student's t-test, one-way ANOVA, or two-way ANOVA with Bonferroni correction. The electrophysiological data were analyzed with two-way repeated measure ANOVA. In all cases, p values were two-tailed, and the comparisons were considered statistically significant when $p < 0.05$. All data are presented as the mean ± s.e.m.

Supplementary Material

Refer to Web version on PubMed Central for supplementary material.

Acknowledgments

We thank Andre Sobel for providing the *Stathmin4A* mutant construct and antibodies against phospho-stathmin, Dusan Bartsch for providing the *htTA* construct, Li-Mei Lin for help with ES work, Monica Mendelson and Mantu Bhaumik for help with generation of mouse strains. We are grateful to Bonnie Firestein, Kim McKim, Chris Rongo as well as members of the Shumyatsky's lab for comments on the manuscript. S.U. was supported by the postdoctoral fellowship from the Japan Society for the Promotion of Science (JSPS). G.P.S. was supported by the National Science Foundation, National Institutes of Health (R01 MH080328), and Whitehall Foundation (#2008-12-104). Research funded in part by the New Jersey Governor's Council for Medical Research and Treatment of Autism, Special Child Health and Early Intervention Services, New Jersey Department of Health and Senior Services.

References

1. Mayford M, Siegelbaum SA, Kandel ER. Synapses and memory storage. Cold Spring Harb Perspect Biol. 2012; 4
2. Hirokawa N, Niwa S, Tanaka Y. Molecular motors in neurons: transport mechanisms and roles in brain function, development, and disease. Neuron. 2010; 68:610–638. [PubMed: 21092854]
3. Hotulainen P, Hoogenraad CC. Actin in dendritic spines: connecting dynamics to function. J Cell Biol. 2010; 189:619–629. [PubMed: 20457765]
4. Gu J, Firestein BL, Zheng JQ. Microtubules in dendritic spine development. J Neurosci. 2008; 28:12120–12124. [PubMed: 19005076]
5. Jaworski J, et al. Dynamic microtubules regulate dendritic spine morphology and synaptic plasticity. Neuron. 2009; 61:85–100. [PubMed: 19146815]
6. Kapitein LC, et al. NMDA receptor activation suppresses microtubule growth and spine entry. J Neurosci. 2011; 31:8194–8209. [PubMed: 21632941]
7. Merriam EB, et al. Dynamic microtubules promote synaptic NMDA receptor-dependent spine enlargement. PLoS One. 2011; 6:e27688. [PubMed: 22096612]
8. Hu X, et al. BDNF-induced increase of PSD-95 in dendritic spines requires dynamic microtubule invasions. J Neurosci. 2011; 31:15597–15603. [PubMed: 22031905]
9. Hu X, Viesselmann C, Nam S, Merriam E, Dent EW. Activity-dependent dynamic microtubule invasion of dendritic spines. J Neurosci. 2008; 28:13094–13105. [PubMed: 19052200]
10. Belmont LD, Mitchison TJ. Identification of a protein that interacts with tubulin dimers and increases the catastrophe rate of microtubules. Cell. 1996; 84:623–631. [PubMed: 8598048]

11. Marklund U, Larsson N, Gradin HM, Brattsand G, Gullberg M. Oncoprotein 18 is a phosphorylation-responsive regulator of microtubule dynamics. Embo J. 1996; 15:5290–5298. [PubMed: 8895574]
12. Di Paolo G, Antonsson B, Kassel D, Riederer BM, Grenningloh G. Phosphorylation regulates the microtubule-destabilizing activity of stathmin and its interaction with tubulin. FEBS Lett. 1997; 416:149–152. [PubMed: 9369201]
13. Larsson N, Marklund U, Gradin HM, Brattsand G, Gullberg M. Control of microtubule dynamics by oncoprotein 18: dissection of the regulatory role of multisite phosphorylation during mitosis. Molecular and cellular biology. 1997; 17:5530–5539. [PubMed: 9271428]
14. Martel G, et al. Murine GRPR and stathmin control in opposite directions both cued fear extinction and neural activities of the amygdala and prefrontal cortex. PLoS One. 2012; 7:e30942. [PubMed: 22312434]
15. Brocke B, et al. Stathmin, a gene regulating neural plasticity, affects fear and anxiety processing in humans. Am J Med Genet B Neuropsychiatr Genet. 2010; 153B:243–251. [PubMed: 19526456]
16. Martel G, Nishi A, Shumyatsky GP. Stathmin reveals dissociable roles of the basolateral amygdala in parental and social behaviors. Proc Natl Acad Sci U S A. 2008; 105:14620–14625. [PubMed: 18794533]
17. Shumyatsky GP, et al. stathmin, a gene enriched in the amygdala, controls both learned and innate fear. Cell. 2005; 123:697–709. [PubMed: 16286011]
18. Saetre P, Jazin E, Emilsson L. Age-related changes in gene expression are accelerated in Alzheimer's disease. Synapse. 2011; 65:971–974. [PubMed: 21425351]
19. Ehlis AC, et al. Influence of a genetic variant of the neuronal growth associated protein Stathmin 1 on cognitive and affective control processes: An event-related potential study. Am J Med Genet B Neuropsychiatr Genet. 2011
20. Newpher TM, Ehlers MD. Glutamate receptor dynamics in dendritic microdomains. Neuron. 2008; 58:472–497. [PubMed: 18498731]
21. Bibb JA, Mayford MR, Tsien JZ, Alberini CM. Cognition enhancement strategies. J Neurosci. 2010; 30:14987–14992. [PubMed: 21068302]
22. Conde C, Caceres A. Microtubule assembly, organization and dynamics in axons and dendrites. Nat Rev Neurosci. 2009; 10:319–332. [PubMed: 19377501]
23. Janke C, Bulinski JC. Post-translational regulation of the microtubule cytoskeleton: mechanisms and functions. Nat Rev Mol Cell Biol. 2011; 12:773–786. [PubMed: 22086369]
24. Jeanneteau F, Deinhardt K, Miyoshi G, Bennett AM, Chao MV. The MAP kinase phosphatase MKP-1 regulates BDNF-induced axon branching. Nat Neurosci. 2010; 13:1373–1379. [PubMed: 20935641]
25. Kuntziger T, Gavet O, Sobel A, Bornens M. Differential effect of two stathmin/Op18 phosphorylation mutants on Xenopus embryo development. J Biol Chem. 2001; 276:22979–22984. [PubMed: 11297553]
26. Correia SS, et al. Motor protein-dependent transport of AMPA receptors into spines during long-term potentiation. Nat Neurosci. 2008; 11:457–466. [PubMed: 18311135]
27. Mitsushima D, Ishihara K, Sano A, Kessels HW, Takahashi T. Contextual learning requires synaptic AMPA receptor delivery in the hippocampus. Proc Natl Acad Sci U S A. 2011; 108:12503–12508. [PubMed: 21746893]
28. Matsuo N, Reijmers L, Mayford M. Spine-type-specific recruitment of newly synthesized AMPA receptors with learning. Science. 2008; 319:1104–1107. [PubMed: 18292343]
29. Liu SJ, Zukin RS. Ca2+-permeable AMPA receptors in synaptic plasticity and neuronal death. Trends Neurosci. 2007; 30:126–134. [PubMed: 17275103]
30. Milnerwood AJ, et al. Early increase in extrasynaptic NMDA receptor signaling and expression contributes to phenotype onset in Huntington's disease mice. Neuron. 2010; 65:178–190. [PubMed: 20152125]
31. Pacchioni AM, Vallone J, Worley PF, Kalivas PW. Neuronal pentraxins modulate cocaine-induced neuroadaptations. J Pharmacol Exp Ther. 2009; 328:183–192. [PubMed: 18840757]
32. Konishi Y, Setou M. Tubulin tyrosination navigates the kinesin-1 motor domain to axons. Nat Neurosci. 2009; 12:559–567. [PubMed: 19377471]

33. Setou M, et al. Glutamate-receptor-interacting protein GRIP1 directly steers kinesin to dendrites. Nature. 2002; 417:83–87. [PubMed: 11986669]
34. Brebner K, et al. Nucleus accumbens long-term depression and the expression of behavioral sensitization. Science. 2005; 310:1340–1343. [PubMed: 16311338]
35. Small SA, Chawla MK, Buonocore M, Rapp PR, Barnes CA. Imaging correlates of brain function in monkeys and rats isolates a hippocampal subregion differentially vulnerable to aging. Proc Natl Acad Sci U S A. 2004; 101:7181–7186. [PubMed: 15118105]
36. Burke SN, Barnes CA. Neural plasticity in the ageing brain. Nat Rev Neurosci. 2006; 7:30–40. [PubMed: 16371948]
37. Lawler S. Microtubule dynamics: if you need a shrink try stathmin/Op18. Curr Biol. 1998; 8:R212–214. [PubMed: 9512407]
38. Melander Gradin H, Marklund U, Larsson N, Chatila TA, Gullberg M. Regulation of microtubule dynamics by Ca2+/calmodulin-dependent kinase IV/Gr-dependent phosphorylation of oncoprotein 18. Mol Cell Biol. 1997; 17:3459–3467. [PubMed: 9154845]
39. Manna T, Thrower DA, Honnappa S, Steinmetz MO, Wilson L. Regulation of microtubule dynamic instability in vitro by differentially phosphorylated stathmin. J Biol Chem. 2009; 284:15640–15649. [PubMed: 19359244]
40. Beretta L, Dobransky T, Sobel A. Multiple phosphorylation of stathmin. Identification of four sites phosphorylated in intact cells and in vitro by cyclic AMP-dependent protein kinase and p34cdc2. J Biol Chem. 1993; 268:20076–20084. [PubMed: 8376365]
41. Marklund U, et al. Serine 16 of oncoprotein 18 is a major cytosolic target for the Ca2+/calmodulin-dependent kinase-Gr. Eur J Biochem. 1994; 225:53–60. [PubMed: 7925472]
42. le Gouvello S, Manceau V, Sobel A. Serine 16 of stathmin as a cytosolic target for Ca2+/calmodulin-dependent kinase II after CD2 triggering of human T lymphocytes. Journal of immunology. 1998; 161:1113–1122.
43. Silva AJ, Paylor R, Wehner JM, Tonegawa S. Impaired spatial learning in alpha-calcium-calmodulin kinase II mutant mice. Science. 1992; 257:206–211. [PubMed: 1321493]
44. Kang H, et al. An important role of neural activity-dependent CaMKIV signaling in the consolidation of long-term memory. Cell. 2001; 106:771–783. [PubMed: 11572782]
45. Abel T, et al. Genetic demonstration of a role for PKA in the late phase of LTP and in hippocampus-based long-term memory. Cell. 1997; 88:615–626. [PubMed: 9054501]
46. Westerlund N, et al. Phosphorylation of SCG10/stathmin-2 determines multipolar stage exit and neuronal migration rate. Nat Neurosci. 2011; 14:305–313. [PubMed: 21297631]
47. Barten DM, et al. Hyperdynamic microtubules, cognitive deficits, and pathology are improved in tau transgenic mice with low doses of the microtubule-stabilizing agent BMS-241027. J Neurosci. 2012; 32:7137–7145. [PubMed: 22623658]
48. Wu QF, et al. Fibroblast growth factor 13 is a microtubule-stabilizing protein regulating neuronal polarization and migration. Cell. 2012; 149:1549–1564. [PubMed: 22726441]
49. Fanara P, et al. Changes in microtubule turnover accompany synaptic plasticity and memory formation in response to contextual fear conditioning in mice. Neuroscience. 2010; 168:167–178. [PubMed: 20332016]
50. Federighi G, et al. Modulation of gene expression in contextual fear conditioning in the rat. PLoS One. 2013; 8:e80037. [PubMed: 24278235]
51. Wang Z, et al. Myosin Vb mobilizes recycling endosomes and AMPA receptors for postsynaptic plasticity. Cell. 2008; 135:535–548. [PubMed: 18984164]
52. Hoerndli FJ, et al. Kinesin-1 regulates synaptic strength by mediating the delivery, removal, and redistribution of AMPA receptors. Neuron. 2013; 80:1421–1437. [PubMed: 24360545]
53. Rao-Ruiz P, et al. Retrieval-specific endocytosis of GluA2-AMPARs underlies adaptive reconsolidation of contextual fear. Nat Neurosci. 2011; 14:1302–1308. [PubMed: 21909089]
54. Clem RL, Huganir RL. Calcium-permeable AMPA receptor dynamics mediate fear memory erasure. Science. 2010; 330:1108–1112. [PubMed: 21030604]
55. Hong I, et al. AMPA receptor exchange underlies transient memory destabilization on retrieval. Proc Natl Acad Sci U S A. 2013; 110:8218–8223. [PubMed: 23630279]

56. Ohkawa N, et al. Motor discoordination of transgenic mice overexpressing a microtubule destabilizer, stathmin, specifically in Purkinje cells. Neurosci Res. 2007; 59:93–100. [PubMed: 17640754]
57. Jin LW, et al. Neurofibrillary tangle-associated alteration of stathmin in Alzheimer's disease. Neurobiology of aging. 1996; 17:331–341. [PubMed: 8725893]
58. Hayashi K, et al. Phosphorylation of the tubulin-binding protein, stathmin, by Cdk5 and MAP kinases in the brain. J Neurochem. 2006; 99:237–250. [PubMed: 16925597]
59. Hara Y, et al. Synaptic distributions of GluA2 and PKMzeta in the monkey dentate gyrus and their relationships with aging and memory. J Neurosci. 2012; 32:7336–7344. [PubMed: 22623679]
60. Witte H, Neukirchen D, Bradke F. Microtubule stabilization specifies initial neuronal polarization. J Cell Biol. 2008; 180:619–632. [PubMed: 18268107]
61. Hellal F, et al. Microtubule stabilization reduces scarring and causes axon regeneration after spinal cord injury. Science. 2011; 331:928–931. [PubMed: 21273450]
62. Martel G, Hevi C, Friebely O, Baybutt T, Shumyatsky GP. Zinc transporter 3 is involved in learned fear and extinction, but not in innate fear. Learn Mem. 2010; 17:582–590. [PubMed: 21036893]
63. Martel G, Hevi C, Kane-Goldsmith N, Shumyatsky GP. Zinc transporter ZnT3 is involved in memory dependent on the hippocampus and perirhinal cortex. Behav Brain Res. 2011; 223:233–238. [PubMed: 21545813]
64. Shumyatsky GP, et al. Identification of a signaling network in lateral nucleus of amygdala important for inhibiting memory specifically related to learned fear. Cell. 2002; 111:905–918. [PubMed: 12526815]
65. Barnes CA. Memory deficits associated with senescence: a neurophysiological and behavioral study in the rat. J Comp Physiol Psychol. 1979; 93:74–104. [PubMed: 221551]
66. Uchida S, et al. Early life stress enhances behavioral vulnerability to stress through the activation of REST4-mediated gene transcription in the medial prefrontal cortex of rodents. J Neurosci. 2010; 30:15007–15018. [PubMed: 21068306]
67. Uchida S, et al. Epigenetic status of Gdnf in the ventral striatum determines susceptibility and adaptation to daily stressful events. Neuron. 2011; 69:359–372. [PubMed: 21262472]
68. Hagihara H, Toyama K, Yamasaki N, Miyakawa T. Dissection of hippocampal dentate gyrus from adult mouse. Journal of visualized experiments: JoVE. 2009
69. Uchida S, et al. Impaired hippocampal spinogenesis and neurogenesis and altered affective behavior in mice lacking heat shock factor 1. Proc Natl Acad Sci U S A. 2011; 108:1681–1686. [PubMed: 21205885]
70. Paxinos, G.; Franklin, KBJ. The mouse brain in stereotaxic coordinates. Academic Press; San Diego: 2001.

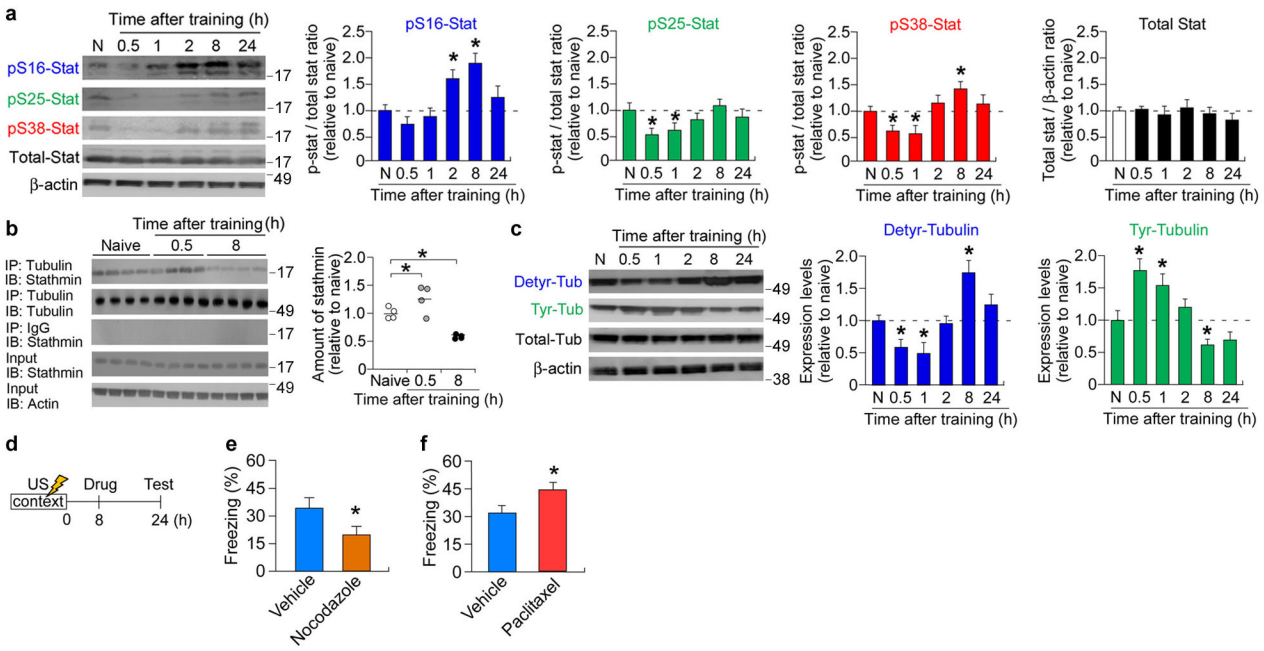

Figure 1. Learning induces biphasic changes in stathmin activity and microtubule stability

(**a**) Immunoblot estimation of stathmin phosphorylation at Ser16 (pS16), Ser25 (pS25), and Ser38 (pS38) 0.5, 1, 2, 8, or 24 h following contextual fear conditioning. N, naïve. $n = 6$ per group (pooled tissues from 3–4 mice per sample). *$p < 0.05$ versus naïve mice (*post hoc* comparison). (**b**) Analysis of stathmin-tubulin protein interactions using co-immunoprecipitation. Stathmin-tubulin complexes are formed at 0.5 h and dissociate at 8 h after contextual fear conditioning. $n = 4$ per group (pooled tissues from 4–5 mice per sample). *$p < 0.05$ (*post hoc* comparison). (**c**) Immunoblot estimation of detyrosinated (Detyr-) and tyrosinated (Tyr-) α-tubulin levels after contextual fear conditioning. $n = 6$ per group (pooled tissues from 3–4 mice per sample). *$p < 0.05$ versus naïve mice (*post hoc* comparison). (**d**) Experimental design for drug administration 8 h following contextual fear conditioning. Memory was tested 24 h after training. (**e**) Mice injected with nocodazole 8 h following training show reduced freezing. vehicle, $n = 11$; nocodazole, $n = 12$. *$p < 0.05$ (Student's t test). (**f**) Mice injected with paclitaxel 8 h following training show increased freezing. vehicle, $n = 11$; nocodazole, $n = 12$. *$p < 0.05$ (Student's t test). Data are expressed as mean ± s.e.m.

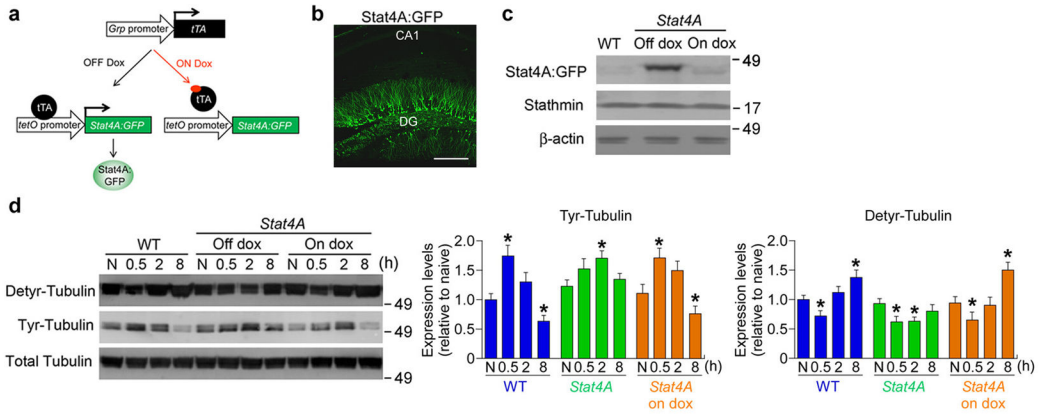

Figure 2. Stathmin phosphorylation is essential for learning-dependent changes in microtubule stability

(**a**) Diagram illustrating transgenic design and control of transgene expression by doxycycline (dox) in *Stat4A* bi-transgenic mice. (**b**) Immunohistochemistry shows that Stat4A:GFP is expressed in the DG, but not CA1 area of the hippocampus. Scale bar, 200 μm. (**c**) Immunoblot using anti-GFP antibody demonstrates that transgene expression is repressed by dox. (**d**) Western blots from the synaptosomal fraction of the DG of *Stat4A* mice show a deficit in microtubule hyperstability at 8 h after contextual fear conditioning. Tyr, tyrosinated tubulin; Detyr, detyrosinated tubulin. N, naïve. $n = 6$ per group (pooled tissues from 3–4 mice per sample). $^*p < 0.05$ versus naïve in corresponding genotype (*post hoc* comparison). Data are expressed as mean ± s.e.m.

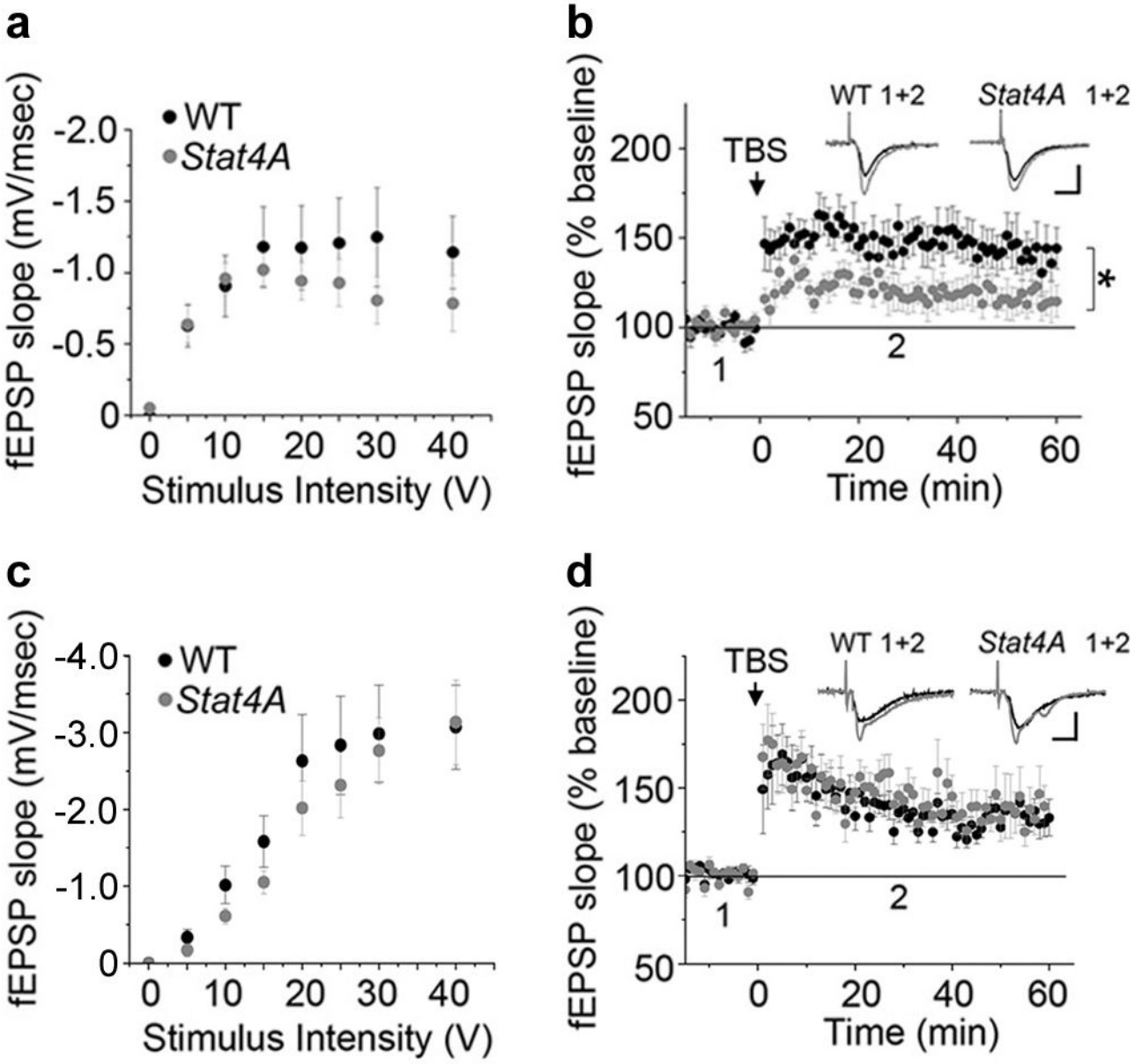

Figure 3. Stathmin phosphorylation is essential for synaptic plasticity

(**a**) Input-output relationship of perforant path to dentate gyrus synaptic responses from wildtype (WT) and mutant mice (n = 4, 6 slices). (**b**) Deficient perforant path to dentate gyrus LTP in *Stat4A* mice (n = 4, 6 slices). (**c**) Input-output relationship of Schaffer Collateral to CA1 (SC-CA1) synaptic responses from WT and *Stat4A* mice. No effect is found on the relationship between stimulus strength and the size of postsynaptic response (input-output relationship). (**d**) *Stat4A* mice show normal LTP at SC-CA1 synapses. Averaged field EPSP data (n = 4, 5 slices). *$p < 0.05$ versus wildtype mice. Data are expressed as mean ± s.e.m.

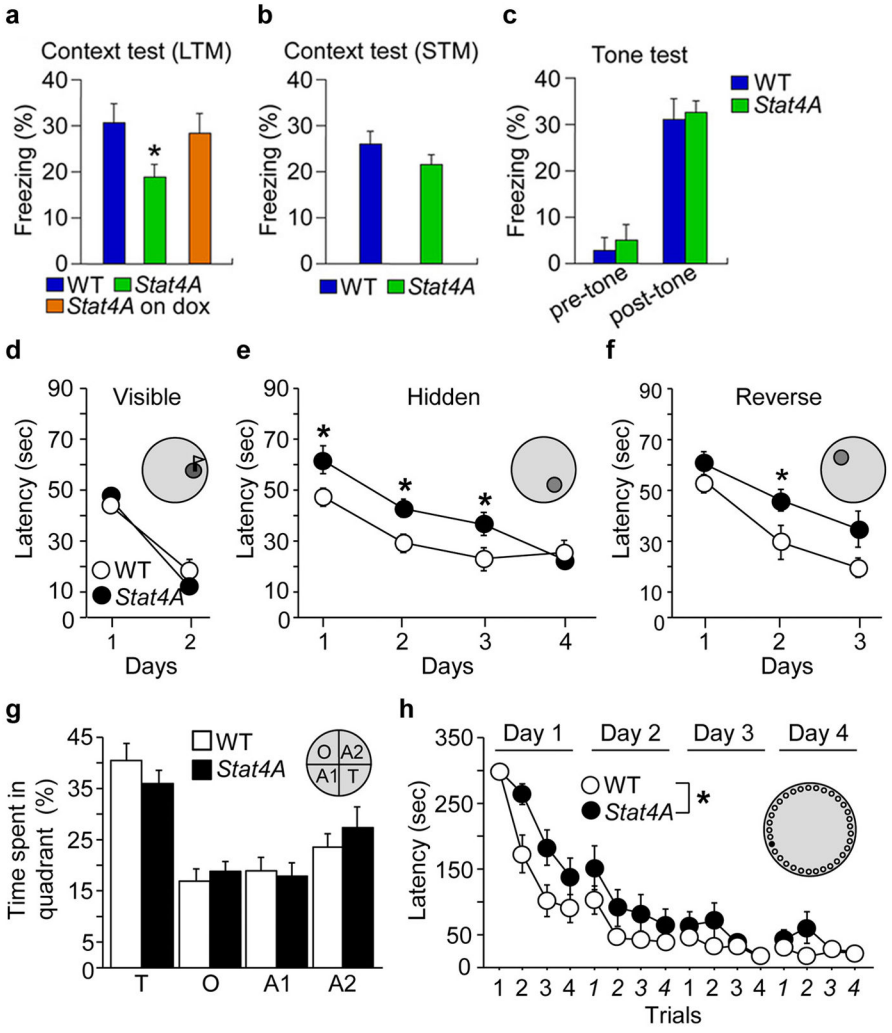

Figure 4. Stathmin phosphorylation is essential for hippocampus-dependent memory

(**a**) Deficient long-term (24 h) contextual fear memory in *Stat4A* mice is rescued by dox. WT, $n = 14$; *Stat4A*, $n = 15$, *Stat4A* on dox, $n = 14$. *$p < 0.05$ versus wildtype mice (*post hoc* comparison). (**b**) Normal short-term (0.5 h) memory in *Stat4A* mice. $n = 10$ per group. (**c**) Cued fear memory is normal in *Stat4A* mice. $n = 14$ per group. (**d–g**) Morris water maze. There was no difference in the visible platform task between the genotypes (**d**). In hidden platform, the latencies of *Stat4A* mice were slower than those of wild-type (WT) mice (**e**). In the reversal learning (transfer task), *Stat4A* mice showed longer latency to find the platform (**f**). The probe trial (**g**) shows normal spatial memory recall in *Stat4A* mice. $n = 10$ for each group. *$p < 0.05$. (**h**) Reduced spatial learning in *Stat4A* mice assessed in Barnes maze. $n = 11$ for each group. * $p < 0.05$. Data are expressed as mean ± s.e.m.

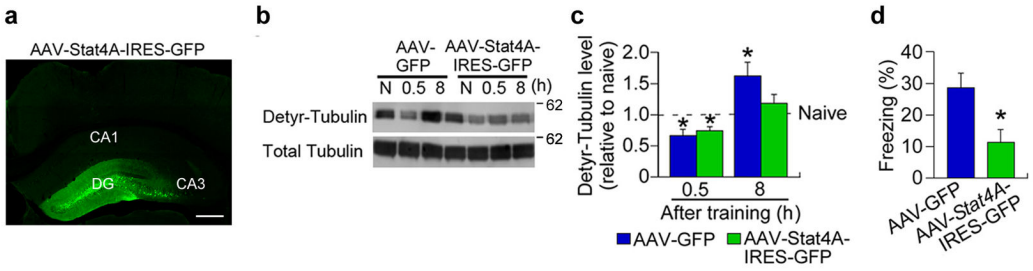

Figure 5. Stathmin control of microtubule stability in the dentate gyrus is critical for contextual fear conditioning

(**a**) AAV-mediated overexpression of *Stat4A* in the dentate gyrus (DG) detected by immunohistochemistry with anti-GFP antibody. Scale bar, 200 μm. (**b,c**) Immunoblot estimation of detyrosinated α-tubulin levels 0.5 h after training in the DG synaptosomal fraction of mice injected with *AAV-GFP* or *AAV-Stat4A-IRES-GFP*. N, naïve. $n = 5–7$ per group (pooled tissues from 3–4 mice per sample). *$p < 0.05$ versus naïve mice (Student's *t* test). (**d**) AAV-mediated overexpression of *Stat4A* reduces contextual fear memory. $n = 11–12$ per group. *$p < 0.01$ (Student's t test). Data are expressed as mean ± s.e.m.

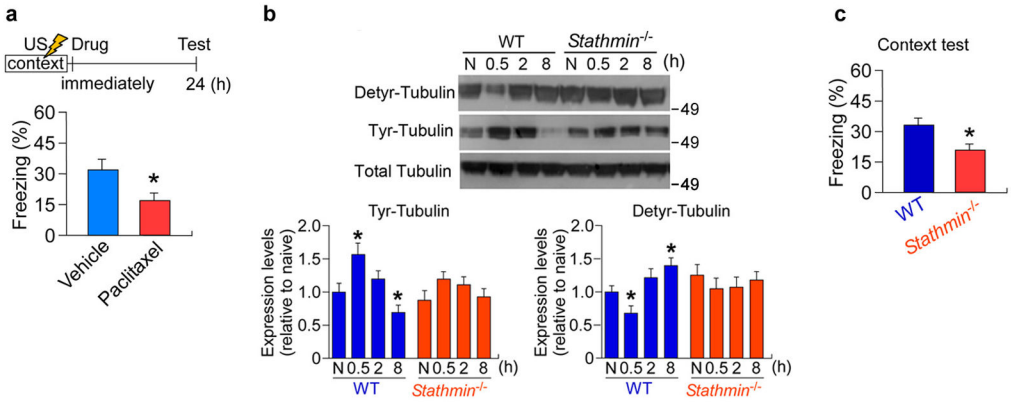

Figure 6. Role of learning-induced microtubule instability in memory

(**a**) Mice injected with paclitaxel immediately following training show reduced freezing. Vehicle, $n = 11$; Paclitaxel, $n = 12$. *$p < 0.05$ (Student's t test). (**b**) s*tathmin*$^{-/-}$ mice show deficit in microtubule destability and stability at 0.5 and 8 h after training. $n = 6$ per group (pooled tissues from 3–4 mice per sample). N, naïve. *$p < 0.05$ versus naïve in corresponding genotype (*post hoc* comparison). (**c**) s*tathmin*$^{-/-}$ mice show reduced long-term (24 h) contextual fear memory. $n = 12$ per group. *$p < 0.01$ (Student's t test).

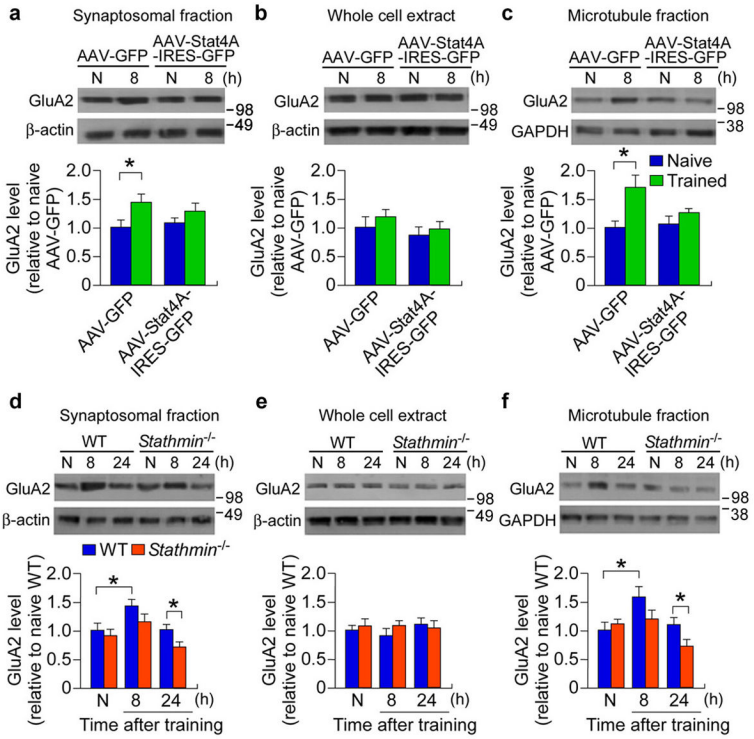

Figure 7. Stathmin regulates learning-dependent dendritic transport of GluA2

(**a–c**) Immunoblot estimation of the level of GluA2 in synaptosomal (**a**, *n* = 8 per group, pooled tissues from 3–4 mice per sample whole cell extract (**b,** *n* = 4 per group) and microtubule (**c**, *n* = 4 per group, pooled tissues from 3–4 mice per sample) fractions of the DG in mice injected with *AAV-GFP* or *AAV-Stat4A-IRES-GFP* in naïve and 8 h after training conditions. **p* < 0.05 (*post hoc* comparison). (**d–f**) Reduced GluA2 synaptic transport in *stathmin*$^{-/-}$ mice, as analyzed by immunoblotting, in the synaptosomal (**d**, *n* = 4 per group, pooled tissues from 3–4 mice per sample), whole cell extract (**e,** *n* = 4 per group) and microtubule (**f,** *n* = 4 per group, pooled tissues from 3–4 mice per sample) fractions in naïve and trained mice. **p* < 0.05 (*post hoc* comparison). Data are expressed as mean ± s.e.m.

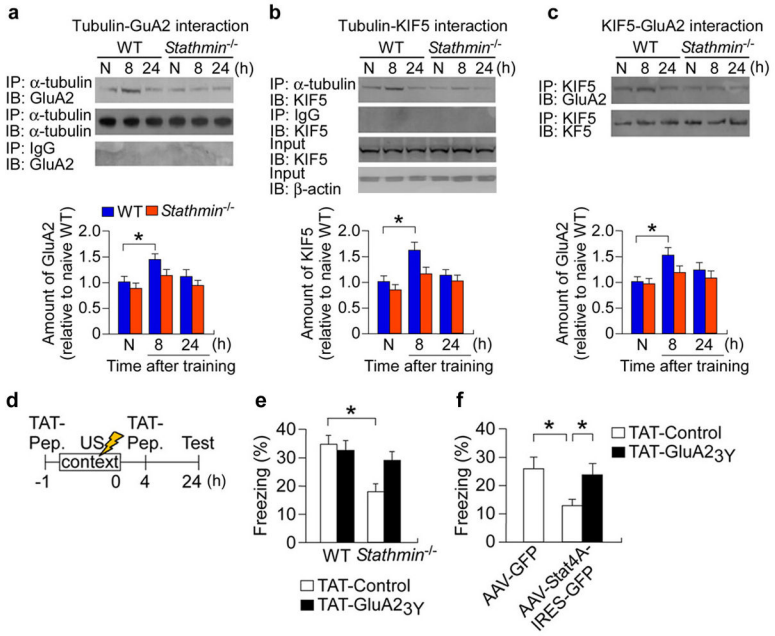

Figure 8. Stathmin controls learning-induced dendritic transport of GluA2 by modulating binding of motor protein KIF5 to microtubules

Co-immunoprecipitation reveals deficiency in protein binding between GluA2 and α-tubulin (**a**), KIF5 and α-tubulin (**b**), and GluA2 and KIF5 (**c**) in *stathmin*$^{-/-}$ mice. N, naïve. $n = 4$ per group (pooled tissues from 2–3 mice per sample). *$p < 0.05$ (*post hoc* comparison). (**d**) Scheme of the experimental design and TAT-GluA2$_{3Y}$ peptide (TAT-Pep.) injection schedule is shown. (**e**) Blocking GluA2 endocytosis by intra-hippocampal injection of TAT-GluA2$_{3Y}$ peptide has no effect in wild-type mice, but rescues contextual fear memory in *stathmin*$^{-/-}$ mice. $n = 12–13$. *$p < 0.05$ versus mice given TAT-control peptide (*post hoc* comparison). (**f**) Rescue of contextual fear memory by TAT-GluA2$_{3Y}$ peptide in wild-type mice injected with *AAV-Stat4A-IRES-GFP*. $n = 10–12$. *$p < 0.05$ (*post hoc* comparison). Data are expressed as mean ± s.e.m.

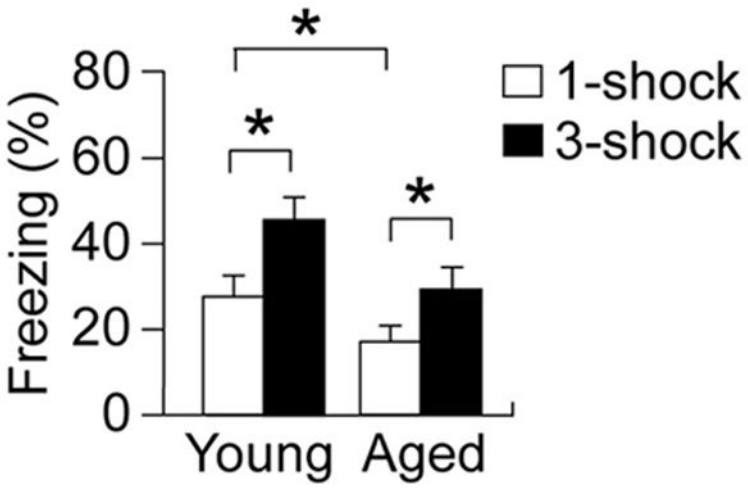

Figure 9. Decreased contextual fear memory in aged wild-type mice

Aged (16–20 month-old) and young adult (2–4 month-old) wild-type mice were subjected to one-footshock or three-footshock contextual fear conditioning. Memory was tested 24 h following training. Aged mice showed reduced contextual fear memory. $n = 11–13$ per group. $p < 0.05$ (*post hoc* comparison). Data are expressed as mean ± s.e.m.

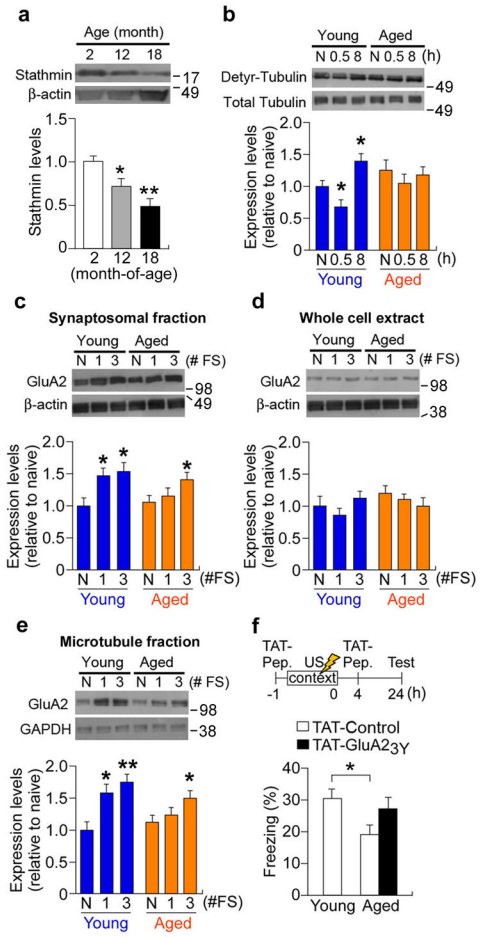

Figure 10. Age-dependent memory loss is associated with microtubule-dependent dendritic transport of GluA2

(**a**) Immunoblot shows reduced level of total stathmin protein in the dentate gyrus (DG) of aged wild-type mice. $n = 5$ per group. *$p < 0.05$, **$p < 0.01$ versus young adult mice (*post hoc* comparison). (**b**) Immunoblot shows deficiency in learning-dependent microtubule destability and hyperstability in aged mice. Detyr, detyrosinated. N, naïve. $n = 5$ per group (pooled tissues from 3–4 mice per sample). *$p < 0.05$ versus naïve young adult mice (*post hoc* comparison). (**c–e**) Immunoblot estimation of GluA2 levels in aged mice in synaptosomal (**c,** $n = 5$ per group, pooled tissues from 3–4 mice per sample), whole cell extract (**d**, $n = 5$ per group), and microtubule (**e,** $n = 5$ per group, pooled tissues from 3–4 mice per sample) fractions of the DG of naïve and trained (single or three foot-shock pairings) aged and young adult mice. N, naïve; #FS, number of foot-shocks; 1, one foot-shock; 3, three foot-shocks. *$p < 0.05$, **$p < 0.01$ versus naive mice in corresponding group (*post hoc* comparison). (**f**) Intra-hippocampal injection of the TAT-GluA2$_{3Y}$ peptide rescued decreased contextual fear memory in aged mice. $n = 12–13$. *$p < 0.05$ (*post hoc* comparison). Data are expressed as mean ± s.e.m.